Parametric Study of High-Velocity Ballistic Impacts on Composite Materials

Megan Hinaus[1], Torodd Berstad[1], David Morin[1], Susanne Thomesen[2], Tore Børvik[1]

[1]Structural Impact Laboratory (SIMLab), Department of Structural Engineering, NTNU – Norwegian University of Science and Technology, Trondheim, Norway
[2]NFM Group, Ski, Norway

Abstract

Ultra-high molecular weight polyethylene (UHMWPE) composites are increasingly used in lightweight, high-performance personal protective equipment for law enforcement and military. Current material performance evaluations rely on experimental testing, which is both time consuming and costly. To address this, numerical simulations using LS-DYNA offer a cost-effective alternative approach, minimizing material waste and reducing experimental testing time.
This study presents a finite element model comprised of UHMWPE composites incorporating independent cohesive layers, based on defined ply properties and estimated interfacial strengths. The simulation utilizes **`*MAT 054-055 (*MAT ENHANCED COMPOSITE DAMAGE)`** for the composite ply layup and **`*MAT 138 (MAT COHESIVE MIXED MODE)`** for the cohesive interfaces. The numerical model was calibrated through comparisons with ballistic experiments, methodically varying ply and cohesive material parameters to evaluate their influence on the simulated residual velocity. Parameters with the most influence were jointly optimized using LS-OPT, with reference to a Recht & Ipson ballistic limit curve from experimental testing, with the resulting model more accurately predicting a numerically simulated ballistic performance.

1 Introduction

Ultra-high molecular weight polyethylene (UHMWPE) fibers, such as Dyneema ®, are becoming increasingly sought after for personal protective equipment in the defense industry due to their high strength and low weight properties [1]. Current industry standards rely on costly and timely physical experimental tests to analyze the behavior of composite plates under high-velocity impacts. Utilizing resources such as finite element modeling software packages like LS-DYNA can drastically reduce the time and costs required for physical experimental testing. The understanding and use of numerical modeling composite materials is essential for the future development of protective materials.
As the first stage of a multi-stage project, this work presents a numerical study in LS-DYNA of high-velocity ballistic impacts on Dyneema ® HB210 plates with the goal of improving the predictability of composites in finite element software. This requires identifying individual key material and contact parameters that most significantly affect the simulation's residual velocity, investigating combinations of material and contact parameters that influence the ballistic velocity, and performing a parameter optimization using LS-OPT to optimize the simulation parameters to experimental data results.
The study combines experimental impact testing on Dyneema ® HB210 composite laminate plates, manufactured and provided by NFM Technology, with a comprehensive sensitivity analysis of the material and contact parameters. Sensitivity investigations assessed individual parameters and combined parameter variations to determine their effect on projectile residual velocity. The identified key parameters were submitted to LS-OPT for calibration between the simulation residual velocity and the experimentally derived ballistic limit curve to create validated and accurate FEA models for UHMWPE composites.

2 Physical Properties of Dyneema ®

2.1 Material Composition

Dyneema ® HB210 is a UHMWPE developed for protective applications in high-impact environments, including ballistic vest inserts, shields, and armored vehicles. Manufactured by Avient Corporation, the "HB" designation refers to the classification of the material as a hard ballistic material, characterized by its rigid resin, giving it suitable high-performance and producing hard armor grade products [2]. On a weight-for-weight basis, Dyneema ® HB210 is 75% lighter and 15 times stronger than steel [1]. The unidirectional composite laminate is oriented in a [0°/ 90°/ 0°/ 90°] ply configuration incorporated with SK99 fibers, optimizing rapid and even energy absorption [3]. Similarly to Dyneema ® HB26 material, Dyneema ® HB210 utilizes the same polyurethane PUR matrix with the same volume fraction [3], [4].

2.1.1 P3 Classification

HB210 composite samples were provided to NTNU by NFM Technology and consisted of two sets of plates, designated P2 and P3. NFM obtained unidirectional Dyneema ® HB210 composite sheets and formed them into plates measuring approximately 250 x 250 x 5 mm. Although the specific details of the plate consolidation process are classified, it is understood that the plate categorizations correspond to the time and duration of temperature and pressure applied to the plates during the consolidation process.
For future reference, this study focuses on the results of the experimental testing and numerical analysis of composite plates formed with the P3 process. Testing and analysis of the composite plates using the P2 process are planned for future work.

3 Experimental Testing

Ballistic experimental testing was conducted on the Dyneema ® HB210 samples to evaluate the residual velocity and determine a ballistic limit of the projectile.

3.1 Test Setup

Experimental testing was conducted at the NTNU Ballistics Laboratory using a setup similar to that described by Eckhoff et al. [3]. Composite samples were mounted on a test rig inside a steel tank, with all four corners clamped to define fixed boundary conditions. One meter away, a Mauser gun was mounted on a tripod and used to fire 1 g, 7 mm-diameter rigid steel sphere projectiles at the center of the composite samples via a remote trigger. Each projectile was fixed to a cartridge case loaded with a calibrated amount of gunpowder to achieve the targeted initial velocity.
All experiments were carried out safely within the enclosed steel tank. A Phantom TMX 7510 high-speed camera, with a frame rate of 230,000 fps, was positioned outside the tank and recorded side views of the impacts through observation windows integrated into the tank wall. The camera recordings were triggered by an acoustic sound sensor initiated by the sound of the gunshot. Impact recordings were post-processed using the Phantom PCC software to extract back-face deformation (BFD) of partially perforated (PP) samples and initial and residual velocities. The layout of the test setup is illustrated in Fig.1:.

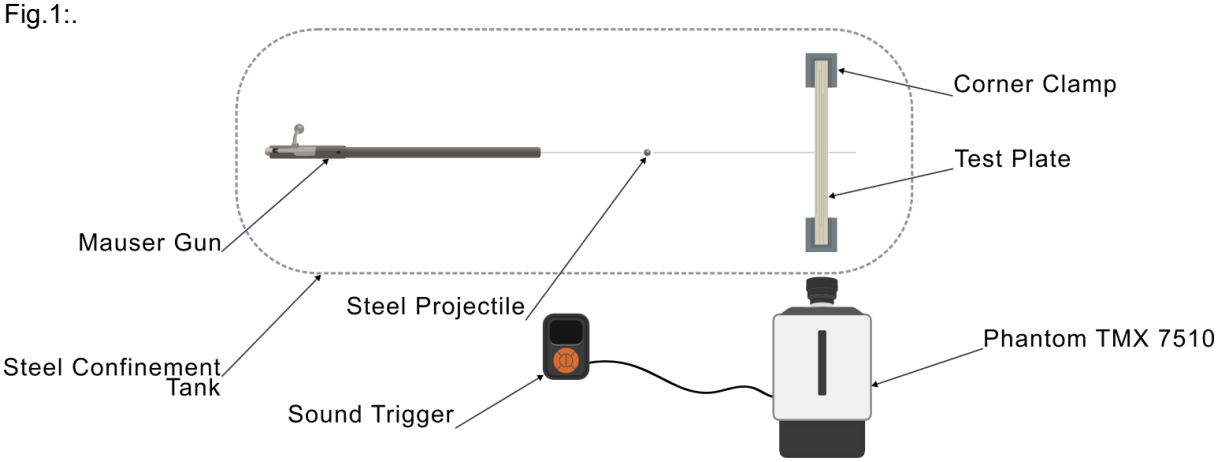

Fig.1: An overview of the test setup to measure the ballistic limit (not to scale).

3.2 Experimental Test Results

Of the 10 HB210 samples tested, initial and residual velocities were recorded successfully for nine. Among these, eight of the tests resulted in a complete perforation (CP) through the composite sample, while one test showed PP. The remaining sample, which also experienced partial perforation, was not successfully recorded with the Phantom TMX 7510 camera.
A partial perforation with an initial velocity of 549.2 m/s was recorded during the HB210 Test 4. The time lapse of the PP impact of Test 4 was extracted using the Phantom PCC software and is presented in Fig.2:. In the first frame, the sphere projectile can be seen approaching the plate followed by the sabot, coming into contact with the composite as a blunt-faced object. Local deformation begins immediately at the impact site, seen at t = 25 µs and continues into frames t = 45 µs and t = 60 µs, where the back fiber fracture also begins to appear. Frames t = 80 µs and t = 110 µs show deformation radiating from the impact site before transitioning to a more global deformation and is seen most clearly at t = 150 µs. The maximum BFD is also observed at t = 150 µs, which was measured to be 15.25 mm with the PCC software. Frame t = 290 µs shows the beginnings of the plate springing back, causing the final

deformation of the plate to reduce. A corresponding cross-sectional view of the impact site is shown in Fig.3:. This includes identified failure modes observed in Test 4, including the expanding fiber fracture from the initial impact, the bulging from the energy transfer of the stopped projectile, and the delamination and cracking around the final resting place of the projectile.

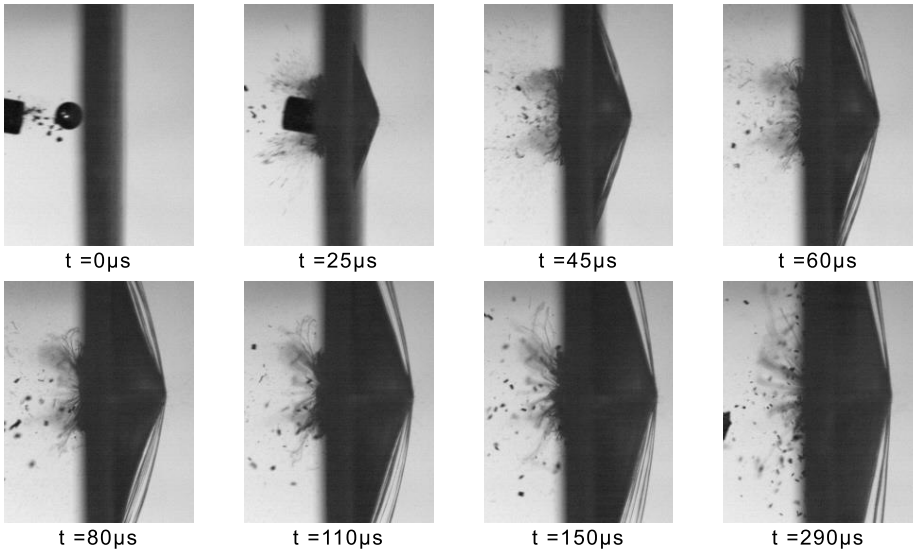

Fig.2: Time lapse of HB210 Test 4 partial perforation with an initial velocity of 549.2 m/s.

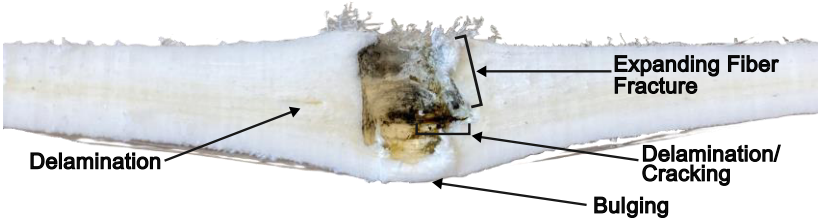

Fig.3: Cross-section of HB210 Test 4 and the failure modes of the PP impact.

From the CP tests, the HB210 Test 10 was selected for visual analysis, having an initial velocity of 549 m/s and a residual velocity of 203.8 m/s. The progression of the impact was extracted from the Phantom TMX 7510 imaging and is shown in Figure Fig.4:. Local deformation due to the initial impact of the projectile is seen from t = 18 µs to t = 35 µs, where the deformation then transitions into global deformation with identified fiber failure at t = 57 µs. The sabot is not seen until = 35 µs and fully until frame t = 57 µs. Upon the projectile exiting the composite by t = 100 µs, an elastic shock wave can be seen when comparing the global deformation of the composite during t = 100, 162, and 214 µs, before snapping back at t = 315 µs. Additionally, Fig.5: displays a cross-sectional view through the impact site, highlighting the failure modes in HB210 Test 10, with expanding fiber fracture, ply delamination, and an exit hole on the back-face.

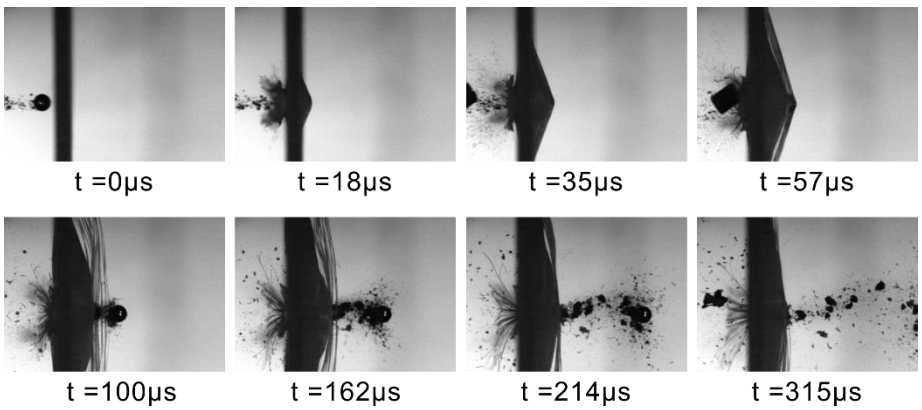

Fig.4: Time lapse of HB210 Test 10 CP with an initial velocity of 594 m/s and a residual velocity of 203.8 m/s.

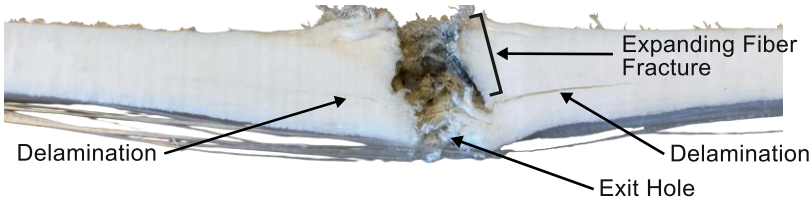

Fig.5: Cross-section of HB210 Test 10 and the failure modes present in the CP impact.

Both Test 4 and Test 10 exhibit expanding fiber fracture and ply delamination approximately 2/3 through the thickness of the plate, as well as edge pull-in to the location of impact. The expanding fiber fracture and failure at this location could potentially be influenced by the sabot in the projectile and cartridge set up; however, current research assumes the sabot does not affect the ballistic properties of the composite plate, as it arrives after the projectile impacts the plate. The bulging BFD in PP Test 4 appears to be more global, due to the energy required to stop the projectile, while CP Test 10 presents a more localized BFD at the exit location of the projectile, with more fiber fracture.

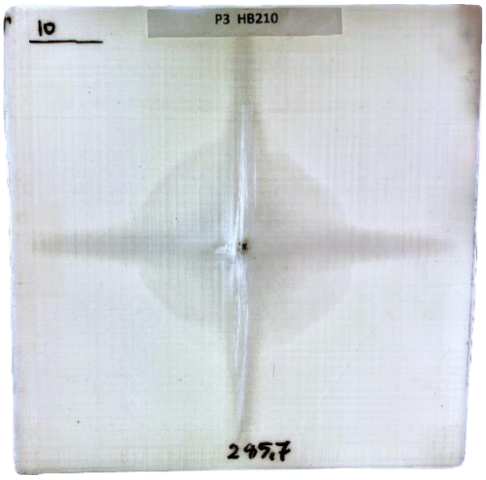

Fig.6: Back-face of HB210 Test 10 post-impact depicting areas of delamination.

Although delamination is present in both analyzed samples, it is not pronounced in the cross-section figures and can be hard to see. An image of the back-face of the Test 10 sample was taken before being cut, shown in Fig.6:. This image better contrasts the delamination throughout the plate. The contrasting highlights and shadows of Test 10 indicate fiber pull-in from the edges and the shadowed circle surrounding the exit hole suggests a higher degree of interlaminar separation than what is visible to the naked eye in Fig.3: and Fig.5:. The lack of delamination seen in Fig.3: and Fig.5: is presumed to be due to the snapback behavior of the plate following impact due to its elastic properties, though cutting process could also influence the visibility in the cross-sections.

3.3 Recht-Ipson Model

Initial and residual velocities were measured with the spatially calibrated TMX 7510 camera using frame-by-frame analysis, and the data points were then used to fit a Recht-Ipson model to the experimental data, as shown in Equation (1). The initial and residual velocities of the projectile are denoted by V_i and V_r, respectively. The ballistic limit, V_{bl}, represents the minimum velocity of the projectile required for the complete perforation of the composite plate. The model includes two constants, p and a. Although p is theoretically 2 [6], it was allowed to vary in this study to better fit the experimental data. The constant a is influenced by the mass of the projectile and the mass of the plug (material removed from the target during perforation). The equation for determining a is provided in Equation (2), where m_p is the mass of the projectile and m_{pl} is the mass of the plug. In this investigation, m_{pl} was assumed to be zero, therefore simplifying a to one.

$$V_r = a\left(V_i^p - V_{bl}^p\right)^{\frac{1}{p}} \quad (1)$$

$$a = \frac{m_p}{m_p - m_{pl}} \quad (2)$$

The optimal fit of the Recht-Ipson model was determined in Python by varying V_{bl} and p and minimizing the sum squares of the residual velocity. Please note that due to limited experimental data, a mixed

zone was not achieved, making V_{bl} an estimation. Only data points with nonzero residual velocity were included in the curve-fitting process. The initial and residual velocity data points and the Recht-Ipson curve fitted for the HB210 tests are plotted in Fig.7:.

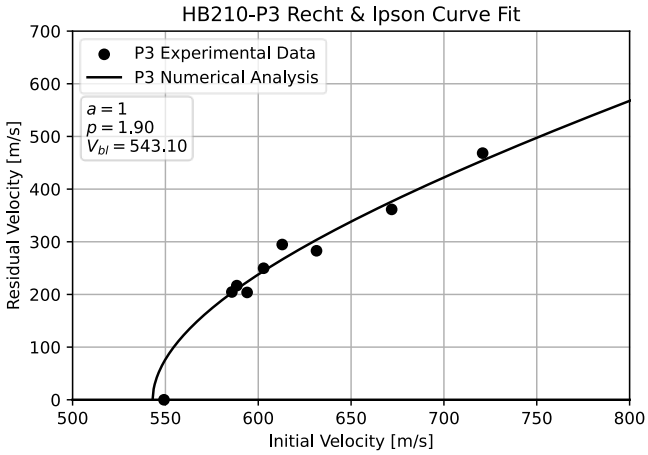

Fig.7: The calculated Recht-Ipson curve and constants from HB210 experimental test data.

4 Numerical Modeling

Numerical simulations were modeled with LS-DYNA, using material properties from sources in literature corresponding to HB210 [3], with the available constitutive material models for composites available in the LS-DYNA software. After simulating the HB210 control model, LS-OPT was used to calibrate certain material properties of the control model to fit the experimental results of HB210.

4.1 Available Constitutive Material Models in LS-DYNA for Composites

LS-DYNA offers a comprehensive selection of nine composite-specific material cards designed to simulate a range of composite behavior. The composite material cards and uses, as defined by Ansys [7] and the LS-DYNA material model manual [8], are listed below:

- **`*MAT 022 (*MAT COMPOSITE DAMAGE)`**: A simplified damage model for composites with options for brittle failure using the Chang-Chang failure model. Best used for preliminary designs with shell and solid elements.
- **`*MAT 054-055 (*MAT ENHANCED COMPOSITE DAMAGE)`**: An enhanced *MAT 022 model, with progressive damage simulation with Chang-Chang or Tsai-Wu failure types, supporting matrix and fiber failure. Supports shell and solid element models. Best used for unidirectional composites under crash and impact loading.
- **`*MAT 058 (*MAT LAMINATED COMPOSITE FABRIC)`**: Used to model unidirectional layers, complete laminates, and woven or braided fabrics. Best for use in shell elements, with the option for solid elements, to model transverse shear damage.
- **`*MAT 059 (*MAT COMPOSITE FAILURE MODEL)`**: A continuum damage, elasto-plastic model, best for tensile failure or pure shear failure. Can be combined with the crashfront model for crash-worthiness situations [9]. Solid elements can be used to model delamination.
- **`*MAT 114 (*MAT LAYERED LINEAR PLASTICITY)`**: An elasto-plastic material to be used for modeling laminated composite shells and sandwich shells [10].
- **`*MAT 116 (*MAT COMPOSITE LAYUP)`**: Used to model elastic response of composite lay-ups with user-defined integration. For use with general composite shell models. The resultant stresses are not calculated, and the model does not use laminated shell theory [10].
- **`*MAT 117 (*MAT COMPOSITE MATRIX)`**: Used for modeling the elastic behavior of pre-integrated shell composites using precomputed matrices to determine the extensional, bending, and coupling stiffness required for the Belytschko-Tsay formulation and assumed strain resultant formulations [10]. The resultant stresses are not calculated.
- **`*MAT 118 (*MAT COMPOSITE DIRECT)`**: Used for modeling elastic behavior of shell ply fiber behavior and response with the precomputed matrices, where the resultants are assumed to be given. The composite thickness must be uniform as the shell thickness is built into the composite model [10].
- **`*MAT 161-162 (*MAT COMPOSITE MSC)`**: An advanced composite model for progressive failure analysis and post-damage softening of layered unidirectional and woven composites

based on the Hashin failure criteria. This model is best used to simulate fiber failure, matrix damage, and delamination under high strain-rate and high-pressure conditions [11]. This material card requires a special license from Material Sciences Corporation.

More information on each composite material card can be found in Volume II of the LS-DYNA User Manual [8].

During this research phase, modeling was performed using solid elements and ***MAT 054-055 (*MAT ENHANCED COMPOSITE DAMAGE)**, based on the progressive damage model from Chang and Chang [12]. The use of this material card allows for accurate simulation of composite failure due to high-velocity ballistic impacts. ***MAT 054-055** is also useful for modeling unidirectional composites, such as HB210, and for modeling in both solid and shell elements.

4.2 Control Material Model

To investigate the delamination of composite plies, one quadrant of the spherical projectile and square composite model was simulated in LS-DYNA, exploiting the biaxial symmetry about the YZ and XZ planes. The modeling process began in LS-PrePost, where two 0.5 mm thick composite layers were manually meshed with biased mesh to enhance the quality of the impact zone.

A shell interface was generated between all elements of the two-ply layers, isolating the shell elements that would lie between the two-ply layers to form a cohesive bonding layer. The shell cohesive interface was then converted into solid cohesive elements with zero thickness. The solid cohesive elements were then copied onto the upper ply, generating a 3D cohesive layer. A volumetric representation of the cohesive layer was necessary to enable future contact definition, which required a defined thickness for proper surface interactions. The cohesive layer was set at 0.0001 mm to remain negligible relative to the overall composite structure.

To construct the full laminate, the ply and cohesive layers were duplicated and alternately stacked until the desired composite thickness was achieved, resulting in a composite with 10 ply layers and 9 cohesive layers. To ensure proper load transfer through the composite, all nodes between the interacting ply and the cohesive faces were merged together.

The composite plies were assigned material keyword ***MAT 054-055 (*MAT ENHANCED COMPOSITE DAMAGE)**, using ***SECTION SOLID ELFORM -2**. The material card was chosen for its ability to model transversely isotropic behavior in unidirectional composites, compatibility with solid elements, and incorporation of the Chang-Chang failure criteria, which account for compressive and tensile failure in the matrix and fibers [12]. The defined ab-plane required for the in-plane material directions corresponded to the global x-y plane of the model. To improve element results with poor aspect ratios, the 8-point hexahedron element type was used. Additionally, ***MAT 000-ADD EROSION** was applied in combination with ***MAT 054-055** to capture material failure and erosion behavior.

The cohesive layers were modeled using material keyword ***MAT 138 (*MAT COHESIVE MIXED MODE)** and paired with cohesive elements defined by ***SECTION SOLID ELFORM 19**.

The projectile was modeled as a solid rigid sphere with a diameter of 7 mm, positioned above the composite model. It was assigned material card ***MAT 020 (*MAT RIGID)** and defined ***SECTION SOLID**
ELFORM -2 elements.

To accurately simulate an impact, multiple contact cards were applied:

- ***CONTACT AUTOMATIC SURFACE TO SURFACE** was applied between the composite ply parts to control contact during impact.
- ***CONTACT TIED SURFACE TO SURFACE** was applied between interacting composite ply and cohesive faces to activate a delamination response in the cohesive layers during impact.
- ***CONTACT ERODING SURFACE TO SURFACE** was applied between the projectile and the composite layup to enable the deletion of elements caused by the excessive erosion due to the high-velocity impact.

Boundary conditions were applied on the x-axis and y-axis to reflect the model's bilateral symmetry. Additionally, to prevent global displacement and replicate the clamped corner conditions used in the experimental setup, the outer corner of the composite, located outside the symmetry conditions, the corner nodes were completely fixed for translation with rotation restricted about the z-axis.

A cross-sectional view of the finalized numerical model, in its initial state, is shown in Fig.8:. To replicate Test 10, the impact shown in Fig.9: was performed with an initial velocity of 594 m/s to assess the accuracy of the model deformation, delamination, and residual velocity. The results of the control model with an initial velocity of 594 m/s produced a residual velocity of 507 m/s and showed that delamination occurred between halfway and two-thirds of the way through the plate.

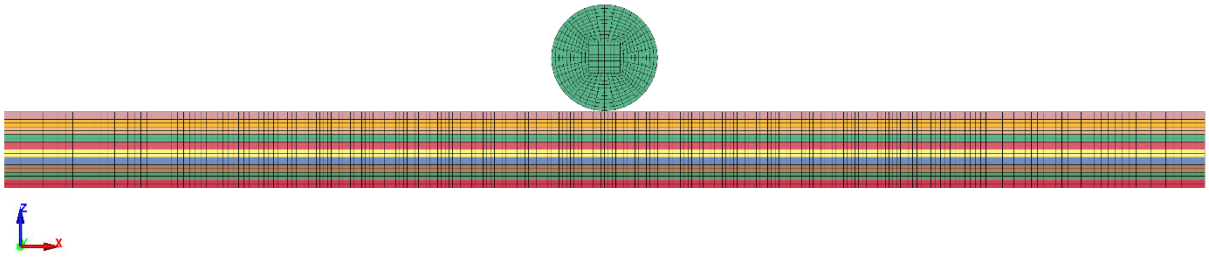

Fig.8: The cross-section of the complete composite model at its initial state reflected about the YZ plane.

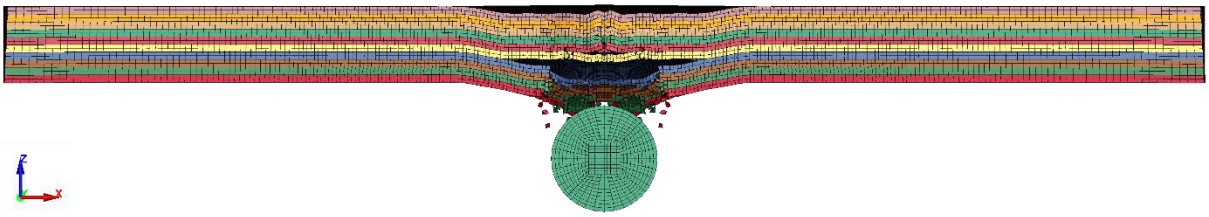

Fig.9: The cross-section of the control model 25 µs after an impact with a 594 m/s initial velocity being reflected about the YZ plane.

With the completion of a simulated impact adhering to the material properties of HB210, an additional series of simulations was run at varying initial velocities, 625 m/s, 675 m/s, 725 m/s, and 775 m/s, to compare the results of the numerical model's performance with the Recht-Ipson model obtained from the experimental tests. The initial and residual velocities generated from these simulations, including the velocities of the Test 10 simulation, are plotted against the Recht-Ipson curve of the experimental data in Fig.10:. The simulation results for HB210, shown in Fig.9: and Fig.10:, deviate significantly from the experimental testing of HB210. Compared to the experiments, the BFD and ply delamination is reduced, and the residual velocities are higher than the Recht-Ipson curve obtained from testing.

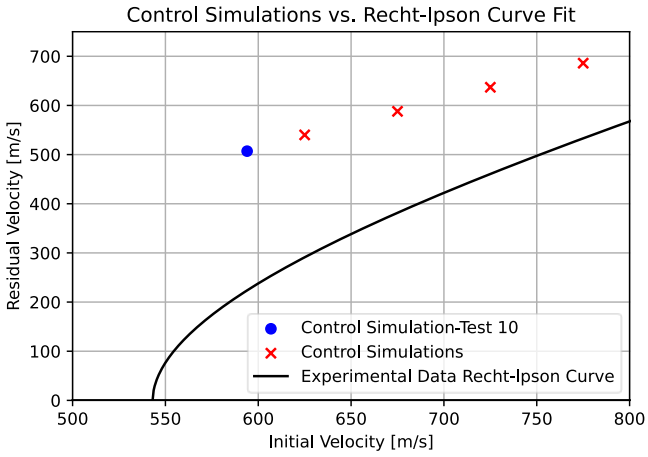

Fig.10: Initial and residual velocities of the control model compared to the experimental data Recht-Ipson curves of HB210 P3.

4.3 Preliminary Parameter Sensitivity Analysis

The residual velocities predicted by the numerical model, described in Section 4.2 and shown in Fig.10: alongside the experimental Recht-Ipson curve, were consistently higher than those measured in the experimental tests. To investigate this discrepancy, sensitivity studies were performed on selected material parameters believed to influence the residual velocity, with the goal of reducing the residual velocity of the numerical simulations to better align with the experimental values. These included parameters from **`*CONTACT`**, **`*MAT 054-055`**, and **`*MAT 138`** keywords. Each parameter investigated was independently varied by a factor of two (doubled and halved) relative to its baseline value in the control numerical model to assess the model's sensitivity to that parameter. All preliminary sensitivity

studies were performed with only one parameter modified per simulation, and each residual velocity result was compared to the control simulation performed in Section 4.2 to determine the percent change. When reviewing a parameter's sensitivity, significant percent changes were determined on the basis of the average percent change between experimental residual velocity data points and their fit to the Recht-Ipson curve. This significance was calculated to be 5%.
The control numerical simulation and all sensitivity studies were performed at an initial velocity of 700 m/s. To match the simulation residual velocities to the Recht-Ipson curve at 700 m/s, a 33% reduction in residual velocity was required.

*4.3.1 Sensitivity Analysis - *CONTACT_ Friction Parameters*

Sensitivity analyses were conducted on the static coefficient of friction (FSa) and dynamic coefficient of friction (FDa) in the ***CONTACT AUTOMATIC SURFACE TO SURFACE** card, as well as the static coefficient of friction (FSe) and the dynamic coefficient of friction (FDe) in the ***CONTACT ERODING SURFACE TO SURFACE** card. The results of these analyses are presented in Fig.11:.
A similar sensitivity analysis was also performed for the coefficients of static and dynamic friction of the ***CONTACT TIED SURFACE TO SURFACE** card. However, there was no change in the residual velocity for either parameter, therefore the parameters and results are omitted from Fig.11:.

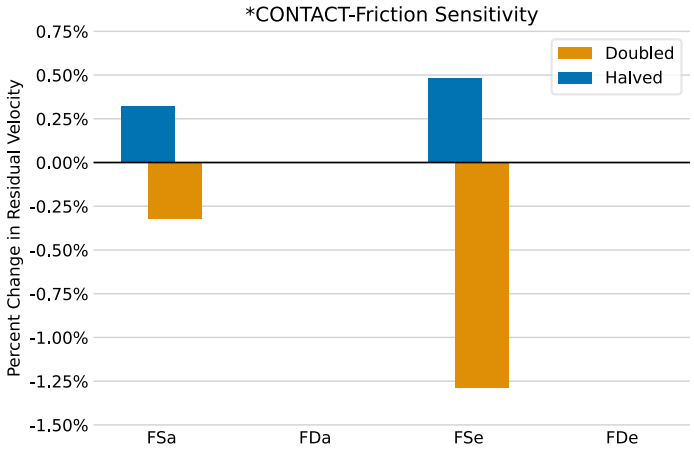

*Fig.11: Percent changes in residual velocity of ***CONTACT** material parameters from the control residual velocity in Section 4.2.*

The results from the ***CONTACT** sensitivity study indicated a decrease in the model's residual velocity when the coefficient of static friction was doubled in both ***CONTACT AUTOMATIC SURFACE TO SURFACE** and ***CONTACT ERODING SURFACE TO SURFACE** keywords, while halving both coefficients of static friction caused a slight increase in residual velocity. In contrast, varying the values of the coefficient of dynamic friction did not affect the residual velocity. The results indicate that there is no significant change in the residual velocity of the model from the ***CONTACT** cards when the friction parameters are varied independently.

*4.3.2 Sensitivity Analysis - *MAT_054-055 Material Parameters*

Material parameters from the ***MAT 054-055** keyword that were identified to have a potential influence on the simulation's residual velocity included Poisson's ratio in the ba plane (PRBA), shear moduli in the ab and bc planes (GAB, GBC), effective failure strain (EFS), longitudinal compressive strength (XC), longitudinal tensile strength (XT), transverse compressive strength in the b axis (YC), transverse tensile strength in the b axis (YT), and shear strength in the ab plane (SC). In addition, the Young's modulus in both the longitudinal direction (EA) and transverse direction (EB) were included in the sensitivity study. Instead of observing the sensitivity changes independently, as with all other parameters, the two Young's moduli were scaled simultaneously in one sensitivity study to remain consistent with the in-plane isotropy properties of the orthotropic control model.

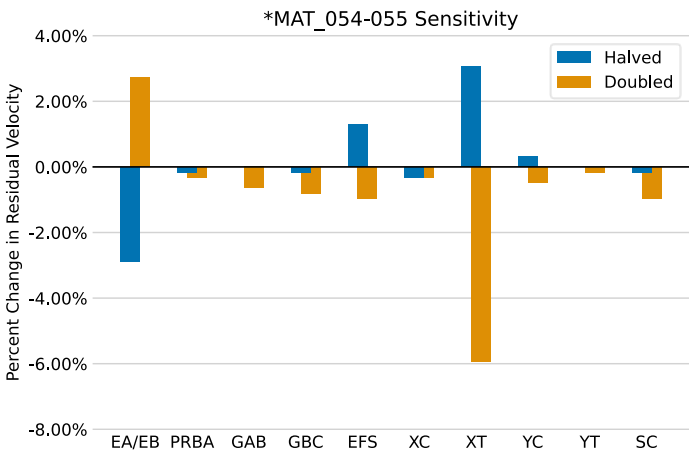

*Fig.12: Percent changes in residual velocity of *MAT 054-055 material parameters from the control residual velocity in Section 4.2.*

The largest changes in residual velocity were observed from variations in the **`*MAT 054-055`** material parameters. As seen in Fig.12:, increasing XT by a factor of two resulted in an approximate 6% decrease in residual velocity. Although changes in XC, YC, and YT produced negligible individual effects, it is likely that their combination with XT could lead to a greater cumulative decrease in residual velocity, as speculated with decreasing EA and EB with the change of other parameters.

4.3.3 Sensitivity Analysis - `*MAT_138` Material Parameters

The cohesive material parameters from material card **`*MAT 138`** identified as influencing the residual velocity in numerical simulations include the stiffness normal to the plane of the cohesive element (EN), the in-plane stiffness of the cohesive element (ET), the energy release rate for normal direction separation (Mode I, GIC), the energy release rate for tangential separation (Mode II, GIIC), the ultimate displacement in the normal direction (UND), and the ultimate displacement in the tangential direction (UTD). Although the peak tractions in both the normal direction (T) and tangential direction (S) were also found to be significant, they are functionally dependent on GIC and UND, and GIIC and UTD, respectively, shown in Equations (3) and (4). Therefore, sensitivity analyses were performed on GIC, GIIC, UND, and UTD, excluding the dependent parameters T and S [8].

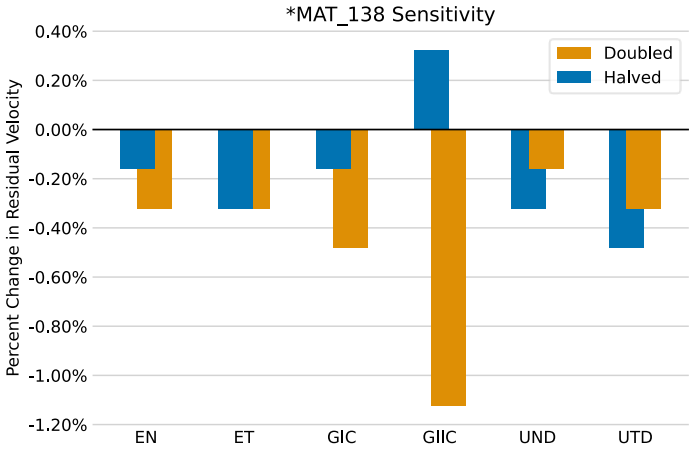

*Fig.13: Percent changes in residual velocity of *MAT 138 material parameters from the control residual velocity in Section 4.2.*

$$T = \frac{2\,GIC}{UND} \tag{3}$$

$$S = \frac{2\,GIIC}{UTD} \tag{4}$$

Seen in Fig.13:, the results of the cohesive material sensitivity study indicated that independent variations of ***MAT 138** parameters had a negligible effect on the residual velocity response of the model. The most notable response occurred when GIIC was doubled, resulting in the greatest decrease in residual velocity. However, this percentage change did not exceed the predetermined threshold for a significant impact as previously defined. Given that GIIC exhibited the strongest influence among the ***MAT 138** parameters, future sensitivity analyses may benefit from exploring combined variations of GIIC and other parameters to further evaluate their collective impact on the residual velocity response.

4.4 Further Parameters Sensitivity Analysis

Following the initial parametric study on individual keywords, additional simulations were conducted to further investigate the parameters according to the results of Section 4.3, recommendations from previous research [3], [13], and information from the LS-DYNA manual. The additional studies examined both individual parameters and combined parameters. Sensitivity ID 1 was developed based on the performance of the friction parameters in Section 4.3.1 and unpublished research by former SIMLab intern Camiel Posthuma [13], who modeled high-velocity ballistic impacts on HB210 material using LS-DYNA in 2024. This study included a specific combination of ***CONTACT AUTOMATIC SURFACE TO SURFACE** and ***CONTACT ERODING SURFACE TO SURFACE** friction parameters presented in Section 4.3.1, with the addition of the viscous damping coefficient (VCD) expressed as a percentage in the ***CONTACT AUTOMATIC SURFACE TO SURFACE** card.
Sensitivity ID 2 further explored the stiffness parameters for ***MAT 054-055**, seen in Section 4.3.2, for PRBA, GAB, and GBC based on material parameters from Posthuma's 2024 report, with the addition of the shear modulus in the ca plane (GCA) [13].
Sensitivity ID 3 evaluated Section 4.3.3's ***MAT 138** cohesive parameters based on the values reported by Eckhoff et al. [3] in his research on the modeling of HB210 in the IMPETUS Solver. The cohesive parameters included input energy release rates for Mode I and Mode II (GIC, GIIC) and peak normal and tangential stresses (T, S). The normal and tangential ultimate displacement values (UND, UTD) were left blank to be automatically calculated by LS-DYNA. In Table 1:, values that were calculated by LS-DYNA are denoted with [-].
Sensitivity ID 4 investigated the softening reduction factor (SOFT) from ***MAT 054-055** Card 5a. The original value used in the control model was based on recommendations from Posthuma's work [13], with the new analysis evaluating the residual velocity response of the model with strengthened crash-front elements.
Sensitivity ID 5 examined the TFAIL criterion (time step for element deletion in ***MAT 054-055** to assess the influence of the time step on failure behavior.
The last two sensitivity studies, IDs 6 and 7, focused on ***MAT 054-055** card's XT and YT, respectively, from Section 4.3.2. The goal of Sensitivity ID 6 and 7 was to investigate the Chang-Chang failure criteria when the parameters of the control model were altered by a factor greater than 2. XT was chosen due to its high influence on residual velocity at 6%, while YT was chosen due to its negligible effect on residual velocity. In these studies, XT and YT were increased by a factor of 10 to assess the effect of extreme changes to the failure criteria.

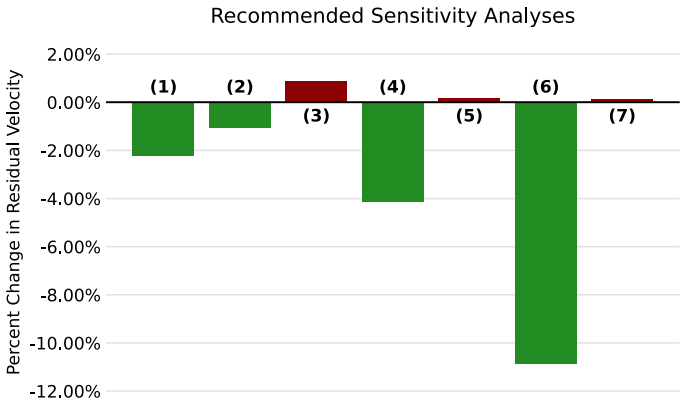

Fig.14: Further sensitivity study percent change in residual velocity compared to the control model in Section 4.2.

All sensitivity IDs and values are provided in Table 1:. The results of the additional sensitivity analyses are shown in Figure 14, Where green indicates a decrease in residual velocity toward the experimentally desired values, and red indicates and increase.

Table 1: Sensitivity IDs and material parameters for additional sensitivity analyses.

ID	LS-DYNA Keyword	Original Value	Analysis Value
(1)	***CONTACT_AUTOMATIC_SURFACE_TO SURFACE FS**	0.3	0.55
	***CONTACT AUTOMATIC SURFACE TO SURFACE FD**	0.1	0.41
	***CONTACT AUTOMATIC SURFACE TO SURFACE VCD**	0 %	20.0%
	***CONTACT ERODING SURFACE TO SURFACE FS**	0.2	0.1
	***CONTACT ERODING SURFACE TO SURFACE FD**	0.1	0.05
(2)	***MAT 054-055 GAB**	0.1738 GPa	0.5 GPa
	***MAT 054-055 GBC**	0.547 GPa	2 GPa
	***MAT 054-055 GCA**	0.547 GPa	2 GPa
	***MAT 054-055 PRBA**	0.0015	0.002
(3)	***MAT 138 T**	- GPa	5.35×10^{-3} GPa
	***MAT 138 S**	- GPa	7.85×10^{-3} GPa
	***MAT 138 GIC**	0.004 kN/mm	5.35×10^{-4} kN/mm
	***MAT 138 GIIC**	0.004 kN/mm	7.85×10^{-4} kN/mm
	***MAT 138 UND**	0.1 mm	- mm
	***MAT 138 UTD**	0.1 mm	- mm
(4)	***MAT 054-055 SOFT**	0.57	2
(5)	***MAT 054-055 TFAIL**	0 ms	0.5 ms
(6)	***MAT 054-055 XT**	1.464 GPa	14.64 GPa
(7)	***MAT 054-055 YT**	1.464 GPa	14.64 GPa

The additional sensitivity analyses, seen in Fig.14:, provided further analysis of the behavior of the model. In Sensitivity ID 1. the increase of the static and dynamic friction coefficients of ***CONTACT AUTOMATIC SURFACE TO_SURFACE** and decrease of the static and dynamic friction coefficients of ***CONTACT ERODING SURFACE_TO SURFACE**, along with the addition of the viscous damping coefficient (VCD) decreased the residual velocity more than any individual friction parameter in Section 4.3.1. The increase in material parameters of ***MAT 054-055** in Sensitivity ID 2 showed a slight decrease in residual velocity but not significantly greater than the decrease of GAB and GBC seen in Section 4.3.2. Modifying the ***MAT 138** cohesive parameters in Sensitivity ID 3 to match literature values caused a slight increase in the residual velocity, the greatest increase from any ***MAT 138** sensitivity study. Increasing the ***MAT 054-055** softening reduction factor (SOFT) in Sensitivity ID 4 produced the second largest residual velocity decrease in the additional studies at approximately 4%. Sensitivity ID 5, which increased the time-step failure criterion (TFAIL), resulted in a negligible increase in residual velocity. Among all parameters tested, increasing ***MAT 054-055** XT by a factor of 10 in Sensitivity ID 6 had the most significant effect, decreasing from 6% to 11%. In contrast, increasing ***MAT 054-055** YT, in Sensitivity ID 7, by a factor of 10, caused a negligible increase in residual velocity.

After observing results with material parameters in Table 1:, the models were further grouped to determine the changes in residual velocity when multiple material parameters or material cards were altered in a model. First, changes in transverse and longitudinal tensile strengths were modeled to determine whether YT could influence the model if combined with XT (IDs 6,7). Additionally, contact parameters, ***MAT 054-055** shear parameters, and ***MAT 054-055** softening reduction factor were grouped together (1,2,4). Lastly, all Sensitivity IDs that decreased residual velocity were combined to attempt to maximize the change in residual velocity (IDs 1,2,4,6,7). The results of these additional studies are shown in Fig.15:.

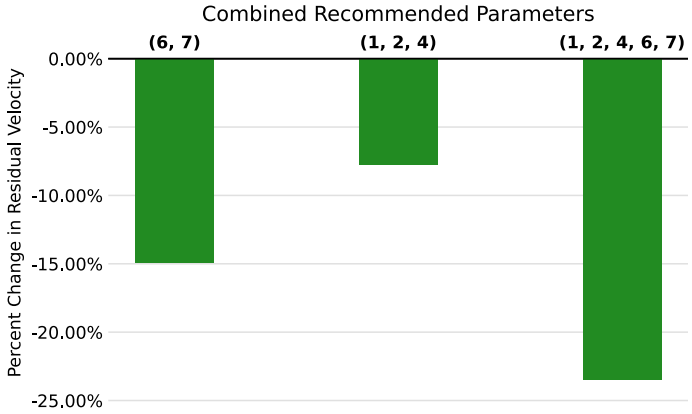

Fig.15: Residual velocity changes of combined sensitivity analyses from Table 1:.

The results of the additional sensitivity studies showed that individual parameters with low residual velocity changes can be combined to better influence the outcome, highlighted by the continued decrease in residual velocity when combining YT with XT. To reflect the experimental velocity in the simulation, the combination of different parameters using differing changes to the control model will be needed to achieve an accurate residual velocity.

4.5 Material Calibration – LS-OPT

Section 4.4 demonstrated that varying combinations of material parameters and their magnitudes can significantly influence the residual velocity predicted by the model. Seven material parameters associated with **`*MAT 054-055`** were selected to be optimized by the LS-OPT software and create a model with an accurate ballistic limit. The parameters include XT, XC, YT, YC, SOFT, and SC directly from **`*MAT 054-055`** and the maximum effective strain at failure (EFFEPS) from the **`*MAT ADD EROSION`** card, which is compatible with the **`*MAT 054-055`** card.

To calibrate these parameters with the experimental Recht-Ipson curve in Fig.7:, four simulations were modeled at different initial velocities, 625 m/s, 675 m/s, 725 m/s, and 775 m/s, in a single file in LS-DYNA. The multi-simulation file, along with the computed Recht-Ipson curve, selected parameters for optimization, and a Python code for percent error were compiled in LS-OPT. The residual velocities with the modifiable parameters from the LS-DYNA file were compared to the Recht-Ipson test curve provided in LS-OPT, and the percent error between the two sets of data guided the iterative optimization of the input parameters. A total of 11 optimization iterations were performed over the course of four days. The final optimized parameters, as defined by the LS-DYNA manual [8], are listed in Table 2: alongside the original baseline values and their respective percent changes.

Table 2: HB210-P3 material calibration, produced by LS OPT.

LS-DYNA Variable	Keyword	Definition	Control Value	P3 Optimized	Percent Change
EFFEPS	**`*MAT ADD EROSION`**	Maximum effective strain at failure [-]	2.5	1.391	-44.36%
XT	**`*MAT 054-055`**	Longitudinal tensile strength [GPa]	1.464	4.151	183.54%
XC	**`*MAT 054-055`**	Longitudinal compressive strength [GPa]	1.464	11.39	678.01%
YT	**`*MAT 054-055`**	Transverse tensile strength [GPa]	1.464	1	-31.69%
YC	**`*MAT 054-055`**	Transverse compressive strength [GPa]	1.464	3.119	113.05%
SOFT	**`*MAT 054-055`**	Softening reduction factor for material strength in crashfront elements [-]	0.57	0.761	33.51%
SC	**`*MAT 054-055`**	Shear strength, ab plane [GPa]	0.065	2.26	3376.92%

Notably, several material parameters exhibited significant changes, including a 678% increase in longitudinal compressive stress (XC) and a 3377% increase in shear strength in the ab plane (SC). While these magnitudes exceed typical and physically realistic material property ranges property ranges, they enable the model to accurately reproduce the experimental ballistic limit curve. Such results indicate that the model does not capture all the physical mechanisms and material properties.
The optimized simulations are shown in Figure 16, which successfully aligned with the Recht-Ipson curve from testing. The residual velocity of the LS-OPT calibrated model, based on the 594 m/s initial velocity of Test 10, was reduced to 271 m/s. The Recht-Ipson curve, defined in Section 3.3, estimates the velocity to be 224 m/s, improving the simulation's velocity by 236 m/s.

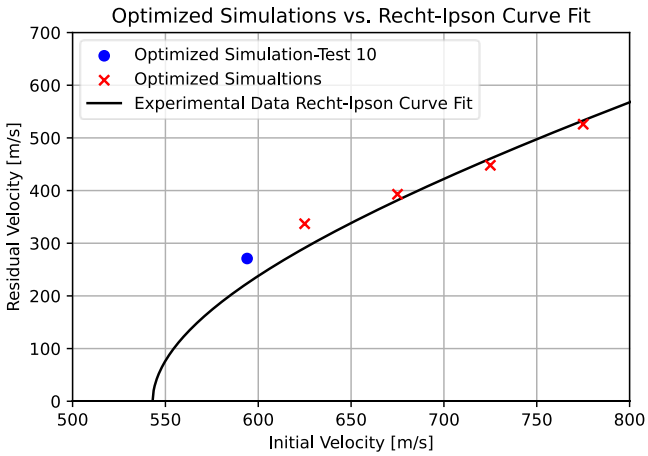

Fig.16: Optimized residual velocity results from LS-OPT compared to the experimental Recht-Ipson curve.

Fig.17: The simulation of Test 10 using material properties calibrated for residual velocity from LS-OPT. The simulation depicts a projectile at 66 µs and an initial velocity of 594 m/s with the model reflected about the YZ axis.

Further comparisons between the original control model with the properties of materials in literature (Figure 9) and the optimized model, shown in Figure 17, revealed more accurate delamination and BFD in the optimized model when compared to the experimental behavior of Test 10 (Figure 4). The optimized simulation also better replicated the shock-wave deformation upon impact observed experimentally, including clearer evidence of edge pull-in. Additionally, the timing of the projectile was more accurate to the experimental data. Full perforation, defined as the moment the projectile completely clears the last layer of the composite, was observed experimentally at 70 µs. In the control simulations, full perforation occurred much earlier, at 25 µs, while the optimized simulation improved the perforation to 66 µs. The only aspect of the simulation that worsened in the optimized model was the location of the delamination. The experimental results indicated that delamination occurred about two-thirds of the way through the thickness of the composite. The control model showed delamination between halfway through and two-thirds of the thickness, whereas the optimized model showed delamination before the halfway point.
Although the optimized model better captured residual velocities and deformation, discrepancies remain between the experimental tests and the numerical simulations. The simulated plate failure produced a larger tear along the y-axis at the impact site, visible behind the sphere projectile in Figure 17, while the

experimental tests produced a circular perforation. The energy ratios were monitored during the control simulation, multi-model simulation, and the final optimized simulation. Both the four-model simulations and the optimized solution produced a slightly increasing energy ratio due to an increase in sliding energy, placing the values outside acceptable limits. Energy ratios continue to be monitored in current research, and future research will focus on improving them without negatively affecting the accuracy of the residual velocity.

5 Summary

Composite testing is primarily conducted through physical experimental tests, which can be costly, but research shows that it is possible to transition much of this testing to digital numerical simulations. LS-DYNA and LS-OPT can be used effectively to calibrate the residual velocity of ballistic impact simulations on composite plates using experimental data. The experimental testing of unidirectional Dyneema ® HB210 composite plates produced a ballistic limit curve that served as the basis for simulation calibration using an LS-DYNA model. Sensitivity studies were performed to assess how changes in material parameters influenced residual velocity. First, studies using individual parameters from *CONTACT, *MAT 054-055, and *MAT 138 keywords evaluated their individual effects on residual velocity. This was followed by additional sensitivity studies that introduced new parameters, modified preliminary studies, and combined material parameters to identify broader trends. Seven material parameters were then selected for optimization in LS-OPT. Using the ballistic limit curve and a Python script, the residual velocities of four models with differing initial velocities were fitted to the experimental results. The simulations with optimized parameters successfully reproduced the experimental Recht-Ipson curve, producing calibrated material parameters. The simulation exhibited more accurate plate deformation and ply delamination, while the calibrated material properties differed significantly from those supplied to LS-OPT. These results demonstrate the potential to shift composite testing from physical experiments toward validated numerical simulations.

Acknowledgements

Special thanks are extended to Camiel Posthuma and Daniel Eckhoff for sharing their insights on composites, testing, and LS-DYNA. Appreciation is also extended to the Valle Scholarship & Scandinavian Exchange Program at the University of Washington for supporting this research.

References

[1] Avient Corporation, "Ballistic vest inserts and shields," 2024. [Online]. Available: https://www.dyneema.com/sectors/law-enforcement-and-military/ballistic-vest-inserts-and-shields.. [Accessed 21 May 2025].

[2] Avient Corporation, "Dyneema® product portfolio," 2024. [Online]. Available: https://www.dyneema.com/design-with-dyneema/dyneema-product-portfolio. [Accessed 21 May 2025].

[3] D. Eckhoff, S. Thomensen, U. Heisserer and T. Børvik, "Ballistic response behaviour of Dyneema HB210® curved armour plates: An experimental and numerical study," *Thin-Walled Structures,* vol. 213, no. 0263-8231, p. 113 265, 2025.

[4] B. Russell, K. Karthikeyan, V. Deshpane and N. Fleck, "The high strain rate response of Ultra High Molecular-weight Polyethylene: From fibre to laminate," *International Journal of Impact Engineering,* vol. 60, no. 0734-743X, pp. 1-9, 2013.

[5] Vision Research (Phantom High Speed), "TMX 7510 Camera," 2025. [Online]. Available: https://www.phantomhighspeed.com/products/cameras/tmx/7510. [Accessed 17 September 2025].

[6] R. Recht and T. Ipson, "Ballistic perforation dynamics," *Journal of Applied Mechanics,* vol. 30, no. 0021-8936, pp. 384-390, 1963.

[7] Ansys Inc., "Composite models in LS-DYNA," 2025. [Online]. Available: https://lsdyna.ansys.com/composite-models/. [Accessed 26 May 2025].

[8] Livermore Software Technology Corporation, "LS-DYNA Keyword User's Manual, Volume II: Material Models," Ansys Inc. , 2023.

[9] K. Schweizerhof, K. Weimar, T. Munz and T. Rottner, "Crashworthiness modeling of composite materials in LS-DYNA," in *Proceedings of the LS-DYNA World Conference*, Detroit, 1998.

[10] Dynamore GmbH, "FEA Newsletter," no. 2, November 2000.

[11] B. Haque, "A Progressive Composite Damage Model for Unidirectional and Woven Fabric Composites," Material Sciences Corporation (MSC), University of Delaware Center for Composite Materials (UD-CCM), 2022.

[12] F. Chang and K. Chang, "A progressive damage model for laminated composites containing stress concentrations," *Journal of Composite Materials,* vol. 21, no. 9, pp. 834-855, 1987.

[13] C. Posthuma, "Ballistic Impact on {UHMWPE} Fiber-Reinforced Composite Plates," 2024.